THE JOURNAL OF PHYSICAL CHEMISTRY C

Article

pubs.acs.org/JPCC

Model for the Mass Transport during Metal-Assisted Chemical Etching with Contiguous Metal Films As Catalysts

Nadine Geyer,[†,*] Bodo Fuhrmann,[‡] Zhipeng Huang,[§] Johannes de Boor,[†] Hartmut S. Leipner,[‡] and Peter Werner[†]

[†]Max Planck Institute of Microstructure Physics, Weinberg 2, D-06120 Halle, Germany

[‡]Interdisciplinary Center of Materials Science, Martin Luther University, Halle-Wittenberg Heinrich-Damerow-Straße 4, D-06120 Halle, Germany

[§]Molecular Materials Research Center, Scientific Research Academy, Jiangsu University, Zhenjiang 212013, People's Republic of China

Supporting Information

ABSTRACT: Metal-assisted chemical etching is a relatively new top-down approach allowing a highly controlled and precise fabrication of Si and Si/Ge superlattice nanowires. It is a simple method with the ability to tailor diverse nanowire parameters like diameter, length, density, orientation, doping level, doping type, and morphology. In a typical metal-assisted chemical etching procedure, a Si substrate is covered by a lithographic noble metal film and etched in a solution containing HF and an oxidant (typically H_2O_2). In general, the function of the metal is to catalyze the reduction of H_2O_2, which delivers electronic holes necessary for the oxidation and subsequent dissolution of the Si oxide by HF. However, the details of the etching process using contiguous metal thin films, especially the mass transport of reactants and byproducts are still not well understood. In this study, the etching mechanism was systematically investigated. Several models of metal-assisted chemical etching using a contiguous metal film as a catalyst were developed and tested by performing different well-controlled etching experiments. The experiments helped to identify two processes fundamental for the formation of Si nanowires. First, a thin porous layer is formed beneath the metal film during etching, which facilitates the transport of the electrolyte (HF and H_2O_2). Second, the porous layer is continuously etched away in an electropolishing process, which occurs in direct contact with the metal film. Our results lead to an improved understanding of the fundamentals of the metal-assisted chemical etching on a microscopic scale. It potentially paves a way to integrate lithography with metal-assisted chemical etching for fabrication of Si nanowires with adjustable surface patterns.

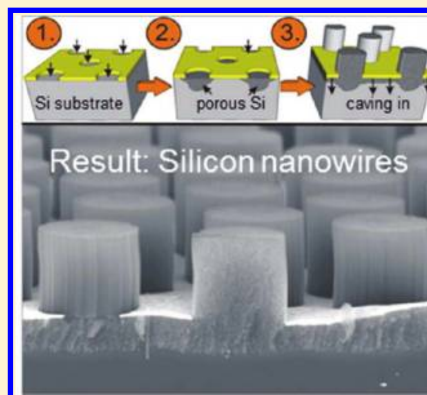

1. INTRODUCTION

Silicon nanowires (SiNWs) and their ordered arrays are attractive structures for potential applications in electronics[1−3] and optoelectronics,[4−6] and appear promising for devising thermoelectric components with a high figure of merit.[7−9] In recent years, a simple metal-assisted electroless etching method using noble metal films as catalyst has been developed and allowed a highly controlled fabrication of vertically aligned crystalline SiNWs[10−12] and Si/Ge superlattices nanowires[13,14] on Si or Si/Ge wafers. This top-down approach involves two steps. First, a structured noble metal film is deposited on the substrate, e.g., via nanosphere lithography. Subsequently, etching in HF and an oxidative agent like H_2O_2,[15,16] $AgNO_3$,[17,18] $KAuCl_4$, or $KMnO_4$[19] is performed. The method yields nanowires with diameters in the range of several μm down to 10 nm. High area densities of 10^{10} wires/cm^2, as well as control of diameter, length, and position of the wires can be achieved.

Despite numerous successful practical applications, the microscopic details of the etching mechanism and of the nanowire formation are still not well understood. A variety of studies have been performed to analyze the formation of porous Si (pSi)[20,21] and the metal-assisted etching mechanism, when a catalyst in the form of metal particles is employed. For the latter, the influence of the type of noble metals used as the catalysts[22−25] (typically Ag, Au, Pd, Pt), doping level,[26−28] doping element, crystallographic orientation of Si substrates, and the concentration of the etching solution[28,29] has been investigated. It is generally accepted that metal-assisted etching is based on local oxidation and dissolution of the Si in HF in the presence of an oxidizing agent, whereas the noble metal catalytically enhances the etching process.[30] The dissolution of the Si beneath the metal proceeds faster than the etching of the remaining areas. The dissolution of the oxidized Si leads to a simultaneous caving in of the noble metal particles into the resulting pores in the Si substrate.[31,32]

Received: April 10, 2012
Revised: May 19, 2012
Published: May 24, 2012

 © 2012 American Chemical Society

The question of how the etching process proceeds on a microscopic scale is still a controversial discussion. Several plausible models have been put forward regarding the etching induced by isolated metal particles,[18,33−36] but no similar investigations for the case of contiguous metal films have been reported so far.

2. THEORETICAL BASIS

In principle, in order to dissolve Si, it is necessary that (i) electronic holes are available in the proximity of the etched region and (ii) a direct contact with the HF electrolyte exists. The latter requirement is important for an effective transport of the reactants and the byproducts of the reaction.

The electronic holes are provided through the reduction of an oxidizing agent (typically H_2O_2, the only example considered in this work) according to Reaction 1:

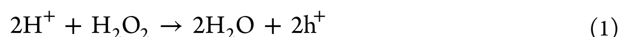

$$2H^+ + H_2O_2 \rightarrow 2H_2O + 2h^+ \quad (1)$$

The generation of electronic holes leads to the oxidation of Si given by Reaction 2:

$$Si + 6H^+ + 6F^- + 4h^+ \rightarrow SiF_6^{2-} + 6H^+ \quad (2)$$

Without any catalytic enhancement, the corresponding etching rate is below 10 nm/h,[37] thus very low. It increases substantially, when a metal (particles or films) is introduced into the system. In this case, the oxidizing agent H_2O_2 is reduced at the top side (not being in the direct contact with the substrate) of the metal, and the resulting holes are injected into the Si beneath the metal particle.

If the catalyst is present as an isolated particle, then the electrolyte can easily penetrate the etching front under the metal; and pores are formed in the semiconductor at the interface to the particle (see Figure 1a). Catalytic etching using extended metal films (see Figure 1b) must be governed by a mechanism different from the catalyst particle case. The electrolyte cannot diffuse easily beneath the extended film. The fundamental question of the mass transport has to be reconsidered. Obviously, it is one of the key issues to control fabrication and properties of SiNWs, most notably their morphology.

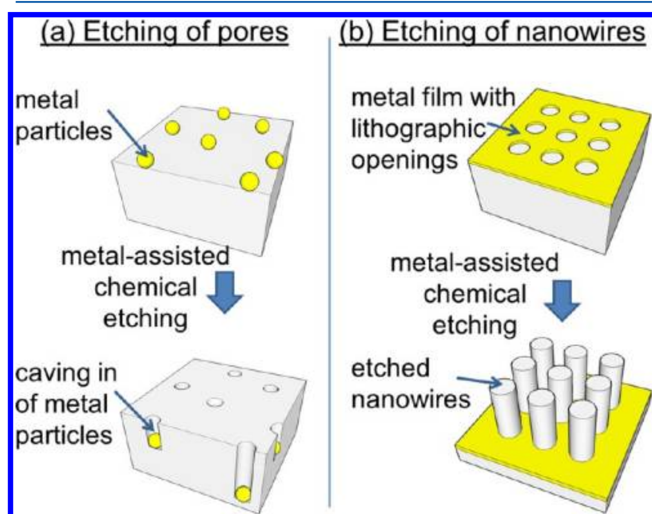

Figure 1. Comparison of possible topologies of the metal film and the corresponding etched structures: (a) isolated metal particles and pores in the Si during metal-assisted chemical etching produced and (b) contiguous metal film with ordered lithographic openings and the resulting nanowire array.

3. EXPERIMENTAL SECTION

In the experiments presented, SiNWs were fabricated by a combination of colloidal lithography, plasma etching, and metal-assisted chemical wet etching. In the experiments, 10 different commercial Si wafers with doping levels from 10^{14} to 10^{19} cm^{-3} (both p- and n-type doped) were cut into (2 × 2) cm^2 pieces and cleaned in a standard RCA I solution containing H_2O_2 (30 wt.%), NH_4OH (25 wt.%), and H_2O solution in a volume ratio of 1:1:5 under 80 °C for 15 min to entirely remove organics. Subsequently, the cleaned substrates were rinsed with deionized water. The well-known fabrication method of SiNWs by metal-assisted etching involves four main steps. First, a monolayer of hexagonally ordered close-packed polystyrene (PS) spheres in diluted colloidal form with diameters of several μm (commercially available from "micro-particles GmbH" as a 10 wt.% solution) were deposited on the surface of the Si substrate. By assembling spheres on a water/air interface, extended areas (several cm^2) of the Si substrate have been covered with PS spheres. Second, this hexagonally close-packed monolayer of monodisperse PS spheres was transferred into hexagonal non-close-packed particle array by means of O_2 plasma etching. The O_2 plasma etching was performed at a flow rate of 400 sccm/min and a pressure of 0.06 mbar for 30 min. By varying the plasma etching time, the diameter of the PS sphere can be easily adjusted. Third, these arrays of modified PS spheres were used as a mask for the subsequent Ag deposition by thermal evaporation. The thickness of the Ag film was varied from 10 to 150 nm. Afterward, the PS spheres were removed by soaking the substrates in a dichloromethane (CH_2Cl_2) bath. This step ended up with a silver mask containing well-defined openings. Fourth, this prestructured Ag film served as a catalyst for the following metal-assisted etching step. For this purpose, the substrate with the structured Ag film was immersed in an etching solution consisting of 5.65 mol/L HF and 0.10 mol/L H_2O_2 in absence of illumination. Finally, the Ag film was removed by immersing the sample in nitric acid for 2 min. At the end, nanowires with diameters ranging from 5 μm to 50 nm and with an aspect ratio up to 10 can be obtained.

4. RESULTS AND DISCUSSION

The geometry of the problem schematically shown in Figure 1b allows to formulate three hypotheses of the diffusion process. They are illustrated in Figure 2: (i) The diffusion of reactants and reaction products occurs through small pores in the metal film, which form in addition to the lithographic openings if the thickness of the metal film is below 15 nm, (cf. Figure 2a, model I). (ii) Diffusion of oxidized and dissolved Si and byproducts takes place in a thin permeable channel formed at the Si/metal interface (see Figure 2b, model II) or (iii) Si atoms diffuse through the metal layer and oxidize and dissolve at the metal/etching solution interface (cf. Figure 2c, model III). The existing literature does not provide enough experimental evidence to support or exclude any of the models. In this work, we aim to fill the gap. We present a series of experiments elucidating the details of the diffusion process during metal-assisted etching of extended films. On the basis of the experimental results, we propose a mechanism for the formation of SiNWs by metal-assisted etching.

dx.doi.org/10.1021/jp3034227 | J. Phys. Chem. C 2012, 116, 13446−13451

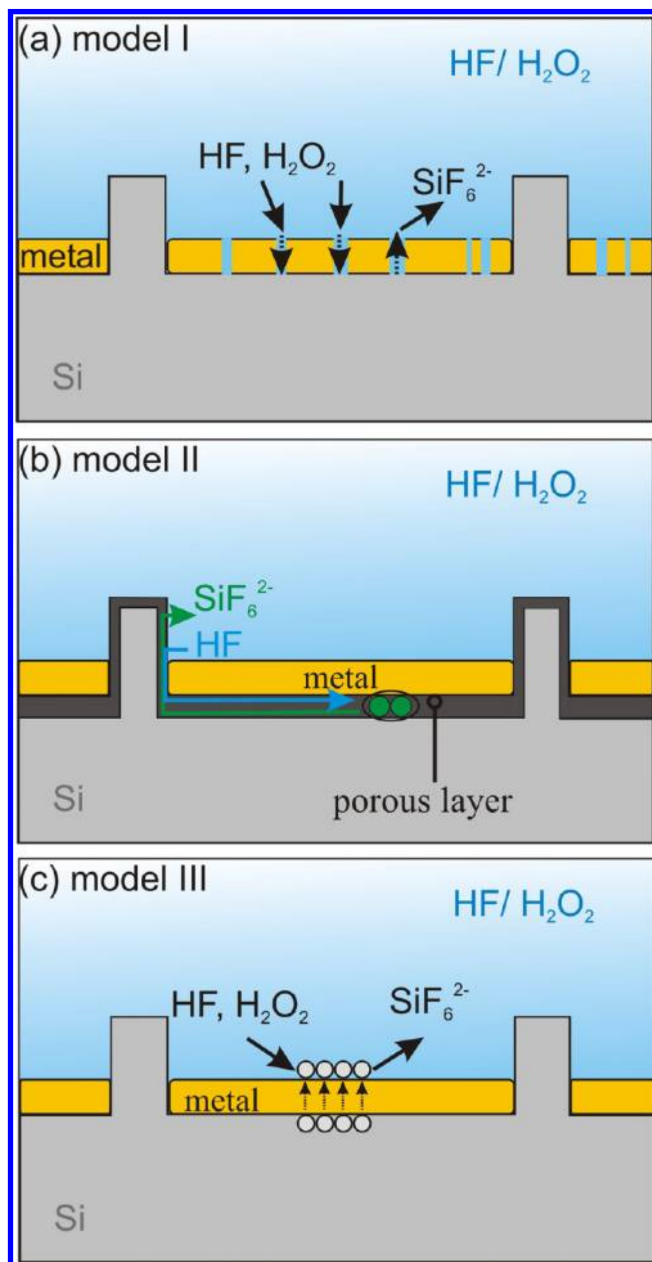

Figure 2. Scheme of possible diffusion processes of the reactants and reaction products during metal-assisted chemical etching. (a) Model I: Diffusion of reactants and reaction products through a porous thin metal film. (b) Model II: The oxidation of the Si surface proceeds at the interface of the metal and the Si substrate by forming a porous silicon layer. Through the porous layer, the HF can diffuse to the bulk Si to facilitate the dissolution. The reactants and the byproducts diffuse as well through the porous layer. (c) Model III: Si atoms diffuse through the metal film and are oxidized at the surface of the metal. Finally, Si is dissolved in form of $[SiF_6]^{2-}$.

To assess the plausibility of model I (i.e., the pores in the thin metal film necessary to permit the electrolyte to reach the etching front at the Si surface), lithographically structured Ag films with different thicknesses varied from 10 to 150 nm were deposited on a Si substrate with different doping levels (10^{16} to 10^{19} cm^{-3}) for both p- and n-type Si substrates. An etching solution containing 5.65 mol/L HF and 0.10 mol/L H_2O_2 was used. Figure 3 shows the resulting wires etched with a thin metal film (thickness of 15 nm, Figure 3a) compared to nanowires etched with a thick film (thickness of 55 nm, Figure 3b).

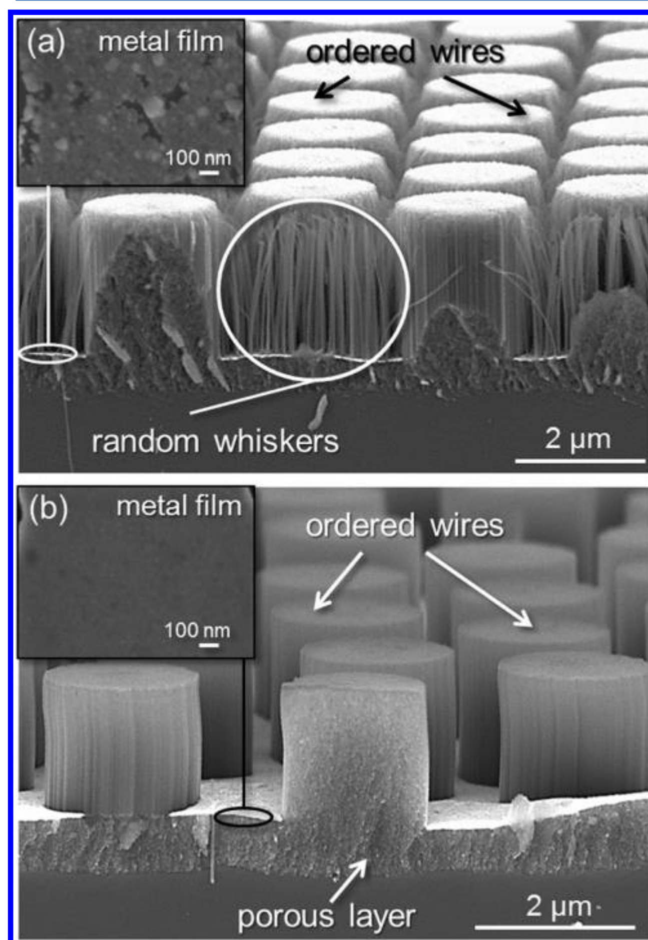

Figure 3. SEM images of Si wires etched using (a) a 15 nm and (b) a 55 nm thick metal film. The etching using thin films with random pores (see inset: top view of 15 nm thick metal film) leads to the formation of disordered nanowires (marked white). With increasing thickness of the metal, closed films (see inset: top view of 55 nm metal film) are obtained, and random nanowires can be avoided. In the two images, the metal film was not removed.

In the case of etching with thin films (containing additional small pores as observed by scanning and transmission microscopy), slender Si whiskers with diameters in the range of 5 to 15 nm are formed in the interstices of the ordered wires with a diameter of 2 μm. The ordered wires are obtained as well using a thick (above 50 nm) Ag film. In this case, the whiskers are not formed. Consequently, a metal film with small pores is not necessary for metal-assisted etching of SiNWs, and model I can be rejected. The experiments described below focus on the proof of models II and III.

With a more careful look, Figure 3 reveals a porous silicon layer beneath the nanowires. Etching experiments have shown that the thickness of this pSi layer depends on the doping level of the Si substrate. For a doping level above 10^{18} cm^{-3}, the thickness of the porous layer is large and amounts to several μm. In this case, the entire NWs are porous.[38,39] In the case of doping below 10^{18} cm^{-3}, a porous layer could be identified by transmission electron microscopy (TEM) too. However, it is much thinner (about 100 nm). In Figure S1 of the Supporting Information (SI), we present NWs etched using a substrate

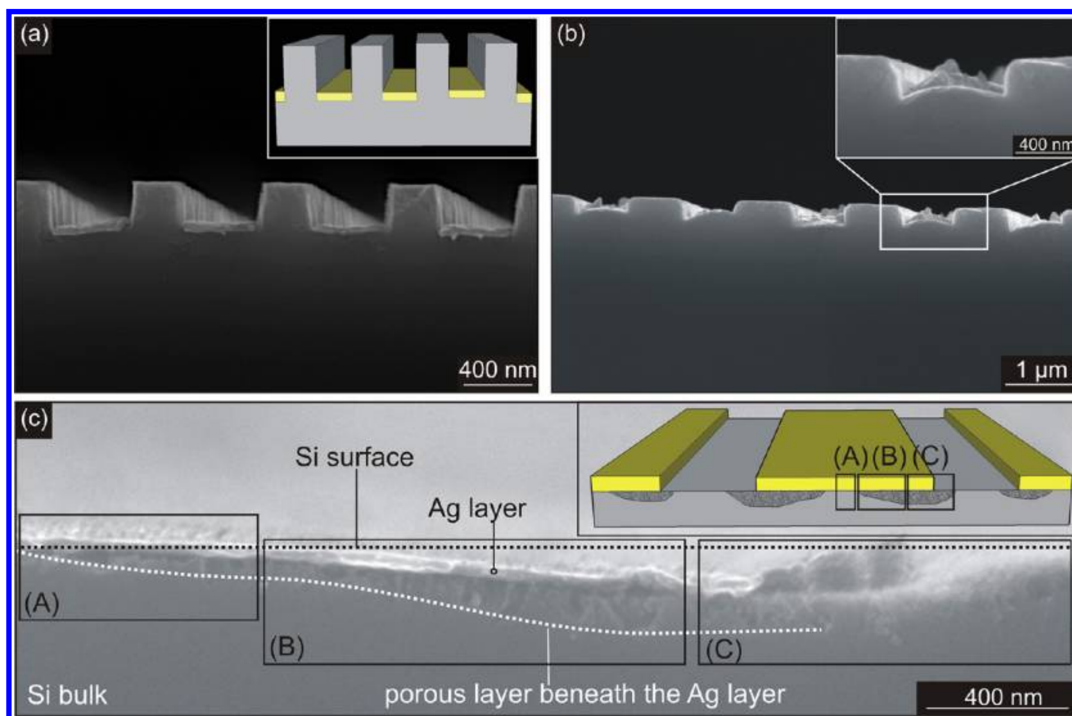

Figure 4. SEM cross section images of etched Ag stripes (etching time: 5 min) with a thickness of 40 nm with different lateral sizes: (a) 390 nm and (b) 710 nm. The etching rate in (a) amounts to 35 nm/min and in (b) 20 nm/min. (c) Detailed view of the edge (position C) to the middle part (position A) of a stripe with the lateral size of 8 μm. The etching rate decreases toward the middle of the stripe because the lateral etching beneath the Ag layer (white line) is not homogeneous.

with a low doping level of 2×10^{14} cm^{-3}. At this low doping level, crystalline SiNWs with a thin pSi surface layer form upon etching. The fact that the porous layer beneath the metal film is always present (for both types of doping) represents an indirect evidence for model II. In addition, the influence of the ambient temperature on the mass diffusion mechanism was investigated. As expected, the growth of the porous layer accelerates at elevated temperatures, which further improves mass transport and enhances etching rate.

Information on the role of the particular diffusion processes in models II and III may be obtained by the investigation of the etching speed as a function of the lateral size and the thickness of the metal layer. The difference between model II and III can be related to the diffusion length of the electrolyte or the dissolved Si. In model II, the diffusion length is determined by the lateral size (distance between the openings) of the metal film, whereas in the case of model III it is given by the thickness of the metal film. If thickness or width of the metal layer is varied, one can distinguish between the two models.

For this purpose two sets of etching experiments were carried out: metal stripes with (i) different lateral sizes, but the same thickness and (ii) identical lateral sizes and varying thickness were deposited onto Si substrate and subsequently etched in HF and H_2O_2. If the etching process proceeds according to model II, then the etching rate should decrease with increasing lateral size of the metal stripes, as the diffusion path for the reactants would increase. However, if the etching occurs according to model III, the etching rate should not depend on the lateral size, but on the thickness of the stripes. For the purpose of the experiments discussed, metal stripes were fabricated by laser interference lithography (LIL)[40,41] or photolithography and thermal evaporation. The first step involves the fabrication of photoresist stripes by LIL. Here, a 200-nm thick photoresist film (AR-N4240, mixed with diluter AR 300−12 at a 1:2 ratio) was spin-coated onto the Si substrate by 4000 rpm for 30 s. Second, the sample was exposed to UV light with a wavelength of 244 nm of a frequency-doubled argon-ion laser (3 mW output power) in a standard Lloyd's mirror interferometer, further details about the setup can be found elsewhere.[39,40] Residual photoresist between the stripes can be removed by an etching step in oxygen plasma at 100 W and a pressure below 2×10^{-9} bar for 30 s. These photoresist stripes serve as a mask for the following thermal evaporation of a 40 nm thick Ag film. The photoresist and its metallic cladding were removed by acetone in an ultrasonic bath for 30 s.

After etching, the metal stripes cave into the Si substrate, which leads to the formation of grooves in the Si substrate. Figure 4 shows scanning electron microscopy (SEM) cross section images of 40 nm thick Ag stripes with lateral sizes of 390 nm (see Figure 4a) and 710 nm (see Figure 4b) after etching. The pictures show clearly different etching rates of stripes with different lateral sizes. More precisely, the etching rate of the 390 nm stripes amounts to 35 nm/min, while the one of the 710 nm stripes to 20 nm/min. Thus, the etching rate decreases with increasing lateral size of the Ag stripes, which supports the mass transport of model II. In addition, metal stripes with different thicknesses but the same widths were deposited on Si substrates. In this case, the etching rate remains constant when the thickness is varied, contrary to the prediction of model III. We performed analogous experiments with metal films featuring ordered circular openings. While the openings of the film were kept of constant size, different thicknesses of metal film were etched for a given fixed time of 5 min. The results are presented in Figure S2 of the SI: the length of the nanowires does not depend on the thickness. The

etching rate depends strongly on the openings widths and distance between wires.

We can conclude that model II is valid: Oxidation and dissolution of Si occurs at the metal/Si interface, even if the lateral size of the metal stripes is on the order of micrometers. For very wide stripes (width between 3 and 12 μm), the etching proceeds faster at the edges than at the middle part of the stripes, see Figure 4c. The reason is the long diffusion path that the electrolyte is required to pass beneath the Ag. If the diffusion length becomes too long (as in Figure 4c), the electrolyte is consumed before the Si area beneath the entire Ag layer is laterally etched. This explains why stripes with widths above 3 μm are bent: The etching rate decreases with an increasing distance from the stripe's edge due to an increasing diffusion length (see inset of Figure 4c). Here, the etching rate at the edge of the stripe amounts to 35 nn/min and at the middle part of the stripe to only 21 nm/min.

If a porous Si layer forms beneath the Ag layer, then the reduction of the H_2O_2 could occur not only on the top side of the metal layer (as the common picture mentioned in the Introduction) but also at the metal/Si interface. To investigate this possibility, the following experiment was devised. Only noble metals like Ag, Au, Pt, and Pd are suitable active catalysts in metal-assisted etching. We established that metals like Cr do not catalyze the reduction of H_2O_2 and do not lead to etching. Therefore, to avoid the reduction of H_2O_2 on the topside of the Ag layer, we additionally deposited a Cr top layer. In this case, the reduction could only occur at the interface and would be impossible if no pSi layer is formed at the interface. In Figure S3a of the SI, we present NWs etched using a pure 40 nm thick Ag layer. Figure S3b of the SI shows a 40 nm thick Ag layer covered with a 20 nm thick Cr layer. In this case, SiNWs form as well. Moreover, the etching rates are similar in both cases. Also in these experiments, a porous layer beneath the Ag layers was detected by TEM, giving supporting evidence for model II.

There are two distinct processes necessary for the formation of SiNWs: (i) the development of pSi and (ii) the removal of the pSi layer (electropolishing) in conjunction with the SiNW formation. For the etching process, it is essential that the electrolyte can reach the interface between the Si substrate and the Ag film. The TEM images in Figure 5 clarify the way metal-assisted etching is facilitated. The starting points of the formation of the pSi are the areas without Ag coverage, i.e., the openings in the Ag mask defined by the lithographic process. The pSi expands isotropically and grows beneath the Ag layer (see Figure 5a−c). This porous layer under the metal allows the electrolyte to diffuse to the Si/Ag interface. In the case of a direct contact of the Ag layer and the Si (without any pSi layer in between) no etching would occur.

With the experimental results presented above, we suggest the following etching mechanism, see Figure 5d. The oxidizing agent H_2O_2 is reduced in HF/H_2O_2 at the surface of the Ag layer according to chemical eq 1[33] owing to the highly active catalytic effect of the Ag layer. Electrons, which are subsequently delivered from the Si, are absorbed from the Ag layer. The delivery of electrons from the silicon valence band is equivalent to the injection of electronic holes h^+ that can diffuse to the Si surface, which is not covered by Ag. In these areas (marked as "D" in Figure 5d), the formation of pSi proceeds according to eq 2.[33] The growth rate of pSi depends on the one hand on the current density (i.e., the number of electronic holes) and on the other hand on the contact with the HF electrolyte. Therefore, pSi is formed first at the edges of the areas "D" (see Figure 5d). The electrolyte is transported beneath the Ag layer through the formed pSi. Owing to the current density distribution of holes at the bulk-Si/electrolyte interface, pSi can expand easily beneath the Ag layer. The pSi layer needs to be continuously removed based on the supply of electronic holes at the Ag/Si interface. Finally, the whole Ag layer sinks into the Si substrate, which leads to the formation of SiNWs.

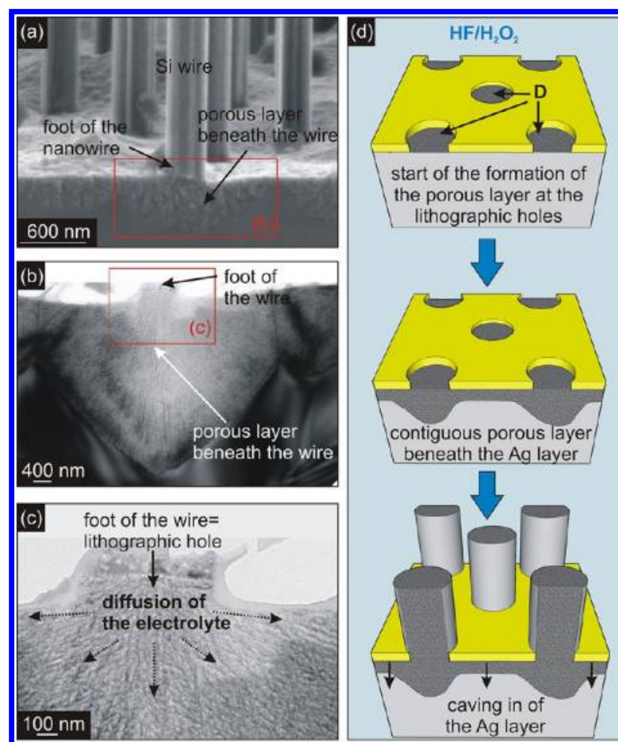

Figure 5. (a) SEM image of the porous area beneath a SiNW and (b) corresponding TEM cross section image. (c) Detailed TEM image of the bottom of the SiNW. The images indicate that the growth of the pSi layer starts at the lithographic openings of the metal film and expands isotropically beneath the entire metal film. (d) Schematic illustration of the process of the formation of SiNWs in metal-assisted etching applied to highly doped Si substrate as starting material.

5. CONCLUSIONS

We have developed and verified a model of metal-assisted etching using a contiguous metal layer as a catalyst. Our experiments have shown that the formation of a porous layer at the Si/Ag interface is a prerequisite for the formation of SiNWs by metal-assisted etching. The mass transport at the Si/metal interface can be described as follows: the etching process forms a thin pSi layer, which permits the exchange of reactants and byproducts of the reaction. The growth rate of pSi depends directly on the doping level of the Si substrate and on the ambient temperature. For highly doped substrates, both SiNWs and the layer beneath the catalyst film are porous. For slightly doped Si substrates, the formation of pSi occurs as well, but the etching process is slower. The resulting SiNWs remain crystalline, with the exception of a thin porous layer at the surface of the wires. The etching process is initiated close to the lithographic openings of the metal film. Si is gradually oxidized and dissolved by HF. If the electrolyte can diffuse along the whole Si/metal interface, then the entire Ag film caves into the Si substrate as a result of the etching. The current density of electronic holes is high enough for an electropolishing only at

positions where the Si is in direct contact with the metal. Consequenty, electropolishing cannot occur in the lithographic openings, which leads to the formation of SiNWs. Our results lead to a deeper understanding of metal-assisted chemical etching and thus to a better experimental control of the top-down fabrication process and the properties of nanowires.

In conclusion, metal-assisted chemical etching allows the fabrication of non-porous SiNWs up to a doping level of 10^{18} cm^{-3}. Nanowires obtained from slightly doped substrates feature a crystalline core and a thin porous outer layer. The latter can be removed, e.g., by an additional HF dip to allow electric contacting. In order to fabricate highly doped non-porous nanowires, they have to be etched first from a slightly doped Si substrate and subsequently doped ex situ by ion implantation or diffusion methods.

■ ASSOCIATED CONTENT

Ⓢ Supporting Information

Figure S1: SEM images of the morphology of etched SiNWs from a slightly doped Si substrate. Figure S2: Length of the wires as a function of metal film thickness. Figure S3: SEM images of etched Si nanowires using Ag and Ag−Cr multilayer films as catalysts. This material is available free of charge via the Internet at http://pubs.acs.org.

■ AUTHOR INFORMATION

Corresponding Author

*E-mail: ngeyer@mpi-halle.mpg.de.

Notes

The authors declare no competing financial interest.

■ ACKNOWLEDGMENTS

Technical support by S. Schlenker (IZM Halle), W. Erfurth (MPI Halle), H. Blumtritt (MPI Halle), S. Hopfe (MPI Halle), C. Münx (MPI Halle), and N. Wollschläger (MPI Halle), as well as funding by the BMBF project "SiGe-TE" are gratefully acknowledged.

■ REFERENCES

(1) Goldberger, J.; Hochbaum, A. I.; Fan, R.; Yang, P. *Nano Lett.* **2006**, *6*, 973.
(2) Schmidt, V.; Riel, H.; Senz, S.; Karg, S.; Riess, W.; Gösele, U. *Small* **2005**, *2*, 85.
(3) Huang, Y.; Lieber, C. M. *Pure Appl. Chem.* **2004**, *76*, 2051.
(4) Tian, B.; Zheng, X.; Kempa, T. J.; Fang, Y.; Yu, N.; Yu, G.; Huang, J.; Lieber, C. M. *Nature* **2007**, *449*, 885.
(5) Agarwal, R.; Lieber, C. M. *Appl. Phys. A: Mater. Sci. Proc.* **2006**, *85*, 209.
(6) Peng, K. Q.; Xu, Y.; Wu, Y.; Yan, Y. J.; Lee, S. T.; Zhu, J. *Small* **2005**, *1*, 1062.
(7) Hochbaum, A. I.; Chen, R.; Delgado, R. D.; Liang, W.; Garnett, E. C.; Najarian, M.; Majumdar, A.; Yang, P. *Nature* **2008**, *451*, 163.
(8) Boukai, A.; Bunimovich, Y.; Tahir-Kheli, J.; Yu, J.-K.; Goddard, W. A.; Heath, J. *Nature* **2008**, *451*, 168.
(9) Hicks, L. D.; Dresselhaus, M. S. *Phys. Rev. B* **1993**, *47*, 16631.
(10) Huang, Z.; Fang, H.; Zhu, J. *Adv. Mater.* **2007**, *19*, 744.
(11) Huang, Z.; Zhang, X.; Reiche, M.; Liu, L.; Lee, W.; Shimizu, T.; Senz, S.; Gösele, U. *Nano Lett.* **2008**, *8*, 3046.
(12) Peng, K. Q.; Zhang, M.; Lu, A.; Wong, N.-B.; Zhang, R.; Lee, S.-T. *Appl. Phys. Lett.* **2007**, *90*, 163123.
(13) Geyer, N.; Huang, Z.; Fuhrmann, B.; Grimm, S.; Reiche, M.; Nguyen-Duc, T.-K.; de Boor, J.; Leipner, H. S.; Werner, P.; Gösele, U. *Nano Lett.* **2009**, *9*, 3106.
(14) Wang, X.; Pey, K. L.; Choi, W. K.; Ho, C. K. F.; Fitzgerald, E.; Antoniadis, D. *Electrochem. Solid-State Lett.* **2009**, *129*, K37.
(15) Huang, Z.; Shimizu, T.; Senz, S.; Zhang, Z.; Zhang, X. X.; Lee, W.; Geyer, N.; Gösele, U. *Nano Lett.* **2009**, *9*, 2519.
(16) Peng, K. Q.; Zhu, J. *Electrochim. Acta* **2004**, *49*, 2563.
(17) Peng, K. Q.; Yan, Y. J.; Gao, S. P.; Zhu, J. *Adv. Mater.* **2002**, *14*, 1164.
(18) Peng, K. Q.; Fang, H.; Hu, J.; Wu, Y.; Zhu, J.; Yan, Y.; Lee, S. T. *Chem.—Eur. J.* **2006**, *12*, 7942.
(19) Hadjersi, T. *Appl. Surf. Sci.* **2007**, *253*, 4156.
(20) Föll, H.; Christophersen, M.; Carstensen, J.; Hasse, G. *Mater. Sci. Eng.* **2002**, *39*, 93.
(21) Smith, R. L.; Collins, S. D. *J. Appl. Phys.* **1992**, *71*, R1.
(22) Yae, S. D.; Abe, M.; Fukumuro, N.; Matsuda, H. *Electrochemistry* **2008**, *76*, 144.
(23) Megouda, N.; Hadjersi, T.; Piret, G.; Boukherroub, R.; Elkechai, O. *Appl. Surf. Sci.* **2009**, *255*, 6210.
(24) Lee, C.-L.; Kanda, Y.; Hirai, T.; Ikeda, S.; Matsumura, M. *J. Electrochem. Soc.* **2009**, *156*, 134.
(25) Fang, H.; Wu, Y.; Zhao, J.; Zhu, J. *Nanotechnology* **2006**, *17*, 3768.
(26) Zhang, M.-L.; Peng, K.-Q.; Fan, X.; Jie, J.-S.; Zhang, R.-Q.; Lee, S.-T.; Wong, N.-B. *J. Phys. Chem.* **2008**, *112*, 4444.
(27) Lee, Y.; Lee, J.; Shul, Y.; Lim, S. *J. Ind. Eng. Chem.* **2008**, *14*, 105.
(28) Hochbaum, A. I.; Gargas, D.; Hwang, Y. J.; Yang, P. *Nano Lett.* **2009**, *9*, 3550.
(29) Dounai, R.; Si-Larbi, K.; Hadjersi, T.; Megouda, N.; Manseri, A. *Phys. Stat. Sol. (A)* **2008**, *205*, 225.
(30) Li, X.; Bohn, P. W. *Appl. Phys. Lett.* **2000**, *77*, 2572.
(31) Tsujino, K.; Matsumura, M. *Adv. Mater.* **2005**, *17*, 1045.
(32) Tsujino, K.; Matsumura, M. *Electrochim. Acta* **2007**, *53*, 28.
(33) Chartier, C.; Bastide, S.; Lévy-Clément, C. *Electrochim. Acta* **2008**, *53*, 5509.
(34) Peng, K. Q.; Lu, A.; Zhang, R.; Lee, S.-T. *Adv. Funct. Mater.* **2008**, *18*, 3026.
(35) Peng, K. Q.; Yan, Y. J.; Gao, S. P.; Zhu, J. *Adv. Funct. Mater.* **2003**, *13*, 127.
(36) Huang, Z.; Geyer, N.; de Boor, J.; Werner, P.; Gösele, U. *Adv. Mater.* **2011**, *23*, 285.
(37) Lehmann, V. *Electrochemistry of Silicon: Instrumentation, Science, Materials, and Applications*; Wiley-VCH: New York, 2002.
(38) Zhong, X.; Qu, Y.; Li, Y.-C.; Liao, L.; Duan, X. *ACS Appl. Mater. Interfaces* **2011**, *3*, 261.
(39) To, W. K.; Him, C.; Li, H.-H.; Huang, Z. *Nano Lett.* **2011**, *11*, 5252.
(40) de Boor, J.; Geyer, N.; Gösele, U.; Schmidt, V. *Opt. Lett.* **2009**, *34*, 1783.
(41) de Boor, J.; Geyer, N.; Wittemann, J. V.; Gösele, U.; Schmidt, U. *Nanotechnology* **2010**, *21*, 095302.